Analysis of silica-filled slot waveguides based on hyperbolic metamaterials

Evgeny G. Mironov,[1,*] Liming Liu,[1] Haroldo T. Hattori,[1] and Richard M. De La Rue[2]

[1]*School of Engineering and Information Technology, UNSW Australia, Canberra, ACT 2610, Australia*
[2]*Optoelectronics Research Group, School of Engineering, The University of Glasgow, Glasgow G12 8QQ, UK*
**Corresponding author: evgeny.mironov@student.adfa.edu.au*

Received April 8, 2014; revised June 3, 2014; accepted June 3, 2014;
posted June 6, 2014 (Doc. ID 209693); published July 10, 2014

We have theoretically studied the optical properties of a filled slot metamaterial waveguide with lateral slab regions consisting of alternating silver–silica multilayers. It is shown that this geometry improves the subwavelength confinement of guided light and that the particular metal–dielectric ratio of 15 nm/10 nm results in substantially enhanced transmission, as compared with metal–dielectric–metal slot waveguides having similar dimensions.

OCIS codes: (160.3918) Metamaterials; (230.7390) Waveguides, planar.
http://dx.doi.org/10.1364/JOSAB.31.001822

1. INTRODUCTION

A general trend in integrated circuit technology is a reduction in the size of components and an increase in speed: In this sense, photonics can provide an ideal platform to reach very high speeds [1]. However, the size of optical devices needs to be considerably reduced to match the size of current nanometric electronic components: One of the main obstacles for reducing the size of optical components is diffraction. In recent years, many different physical phenomena have been used to reduce the size of optical components, such as the photonic bandgap effect [2–7], total internal reflection in high-index contrast structures [8–11], and the excitation of plasmonic waves [12–19]. Compared with the photonic bandgap effect and total internal reflection, plasmonics offers the most promising technology to create ultracompact devices, but one of the main constraints with plasmonics is the optical loss in the metal. In addition to creating very compact devices, very strong confinement of light is useful for trapping and manipulating nanoparticles and biomolecules [20,21].

After light is generated and eventually processed in an optical chip, it must be transported to different regions in the chip by optical waveguides. In contrast with electrical wires, optical waveguides can transport information at very high rates [22]. In general, photonic crystal [23] and total internal reflection [24] waveguides can reach distances above 100 μm with acceptably small propagation loss. If transmission of light over longer distances is needed, light can be coupled to optical fibers by using, for example, grating couplers [25]. If light needs to be confined in tighter spaces, then plasmonic waveguides can be used, in spite of their significantly higher losses [26–29]. In particular, slot waveguides are attractive because they can confine light in very small spaces, which is useful in a wide range of applications in nonlinear optics [30].

Dielectric slot waveguides were first demonstrated by Almeida *et al.* [30] and typically have a gap that is several tens of nanometers in width. These waveguides are used with guided modes that have their main electric field component directed across the slot. Strong electromagnetic confinement (i.e., the strong localization of the electric field) is obtained in such structures because the normal component of electric flux density D is continuous at the slot–cladding interface. (The term "cladding" is used in the present context to identify the regions immediately on either side of the slot. In a "conventional" air-filled slot waveguide, the regions adjacent to the slot essentially form a twin-core waveguide structure, with a small gap between the two cores.) However, purely dielectric slot waveguides still have some mode leakage, particularly when the light is coupled from a conventional stripe waveguide into the slot waveguide. On the other hand, the presence of metal [as in a metal–dielectric–metal (MDM) waveguide] can increase absorption losses, thereby reducing the transmitted power. In the latter case, the optical radiation is transferred by surface plasmon polaritons (SPPs) propagating along the metal–dielectric interface. It is also possible to guide light by exciting long-range SPP, with typical propagation losses of several dB/cm at infrared frequencies. However, this requires construction of a symmetric geometry in which a nanometer-thick metallic film is placed between two adjacent cladding dielectric layers [31,32].

In this paper, we analyze a silica-filled slot waveguide in which the gap is surrounded by two high-index layered hyperbolic metamaterial regions. First, we consider the optical properties of the slot waveguide by varying its geometrical dimensions and metallic volume fraction. Then we investigate the coupling between the proposed slot waveguide and a conventional stripe waveguide. And finally, we study the modal electric field profiles in order to evaluate the modal confinement inside the slot. We show that the slot waveguide provides a balanced solution through simultaneously having high modal effective refractive index and usefully low propagation losses. Additionally, we find that, if the metal and dielectric thicknesses in the lateral slab regions are chosen in the correct ratio, the power transmission is nearly 3.5 times

higher than for the purely plasmonic waveguide of the same dimensions, and, at the same time, the wave confinement significantly improves in comparison with the pure dielectric slot waveguide, e.g., one made with silicon.

2. BACKGROUND INFORMATION

A typical slot waveguide is formed by a narrow low-index slot placed between two high-index slab regions. In the proposed geometry (Fig. 1), these slab regions are constructed from hyperbolic metal–dielectric metamaterials that are capable of supporting large wave vectors (i.e., exhibit large modal effective refractive index values). Each hyperbolic metamaterial region consists of ten alternating silver–silicon pairs with a period of $P = 25$ nm [26]. The surrounding medium (including the slot) is filled with silica ($n_{SiO_2} = 1.444$), and the waveguide is designed to operate at 1550 nm. A practical benefit of embedding the structure in silica is that it prevents the silver inclusions from oxidation. According to the Maxwell–Garnet theory, the components of the anisotropic homogeneous permittivity tensor can be calculated as [33,34]

$$\varepsilon_x = \varepsilon_z = f_{\mathrm{Ag}}\varepsilon_{\mathrm{Ag}} + (1 - f_{\mathrm{Ag}})\varepsilon_{\mathrm{Si}}, \tag{1}$$

$$\varepsilon_y = \frac{\varepsilon_{\mathrm{Ag}}\varepsilon_{\mathrm{Si}}}{f_{\mathrm{Ag}}\varepsilon_{\mathrm{Si}} + (1 - f_{\mathrm{Ag}})\varepsilon_{\mathrm{Ag}}}, \tag{2}$$

where the directions of the axes are shown in Fig. 1, f_{Ag} is the metal filling factor, and $\varepsilon_{\mathrm{Si}} = 12.447$ is the permittivity of silicon. The Maxwell–Garnet theory is valid when (a) the thickness of the metal–dielectric pairs is significantly smaller than the wavelength of interest (each layer is only a few nanometers thick, which is considerably smaller than the optical wavelength) and (b) the scattering from the incursions is low, which implies a low density of conducting domains [35]. Although the formulas have their limitations, they provide physical insight into the results, and, nevertheless, the model discussed is still only a mathematical approximation for the calculation of the complex permittivity.

The permittivity of silver is modeled using the Drude model:

$$\varepsilon_{\mathrm{Ag}}(\omega) = \varepsilon_\infty - \frac{\omega_p^2}{\omega^2 - i\omega\gamma_c}, \tag{3}$$

where $\varepsilon_\infty = 5$ is the background dielectric constant, $\omega_p = 1.38 \times 10^{16}$ rad/s is the plasma resonance frequency, and $\gamma_c = 5.07 \times 10^{13}$ rad/s is the collision frequency [36]. The effective permittivity components ε_x, ε_y, and ε_z as a function of the wavelength for $f_{\mathrm{Ag}} = 0.6$, calculated using the Maxwell–Garnet theory are presented in Fig. 2.

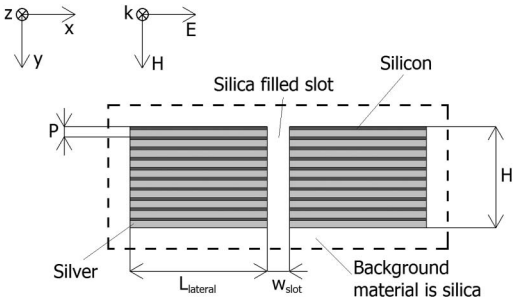

Fig. 1. Slot waveguide cross section.

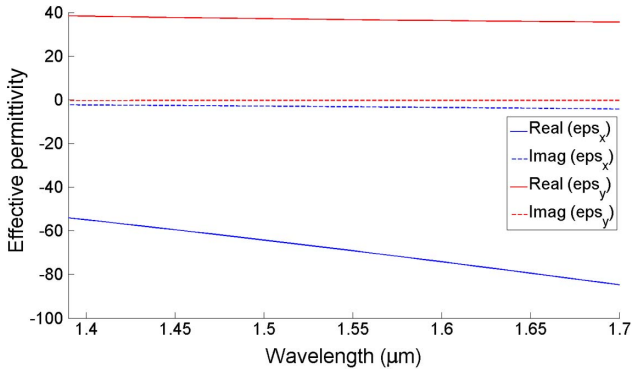

Fig. 2. Effective dielectric permittivity of the slab metal–dielectric regions ($f_{\mathrm{Ag}} = 0.6$) calculated using the Maxwell–Garnet theory [33,34].

The slot waveguide can be considered as being the result of two separate slab waveguides placed close to each other. Each adjacent slab metal–dielectric region can support an eigenmode and, therefore, their coupling results in the formation of either symmetric or antisymmetric modal profiles in the slot waveguide [30]. If the modal profile is symmetric, then the electric field strength inside the slot is amplified and the wave is strongly confined, while, for the antisymmetric mode profile, the opposite electric fields cancel each other and the optical confinement is relatively weak (Fig. 3). As mentioned earlier, in this geometry, only modes with their main component of electric field directed across the gap (the x axis in Fig. 1) are strongly confined inside the slot. Modes that have their main electric field component parallel to the faces of the gap (the y axis in Fig. 1) leak away and rapidly decay [26]. Therefore, only the quasi-TE_{00} modes (with, primarily, field components E_x, H_y, E_z) of this filled slot waveguide are considered in the discussion. Although quasi-TE modes may contain a residual longitudinal mode component of the electric field, its magnitude is considerably weaker than those of the transverse field. The first subindex refers to the number of nodes along the x direction, while the second subindex refers to the number of nodes along the y direction.

For the quasi-TE_{00} coupled mode of a slot waveguide with the width of the lateral slab metal–dielectric region denoted by L_{lateral} and the width of the slot by w_{slot}, the main electric field component inside the gap can be written as [30]

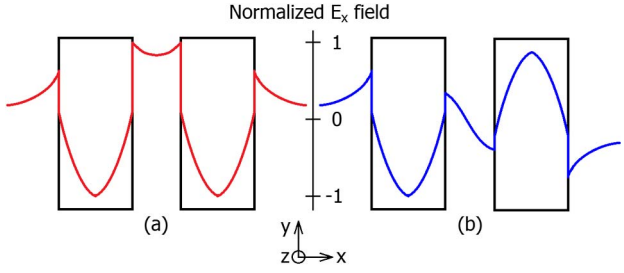

Fig. 3. Electric field profiles for (a) symmetric and (b) antisymmetric modes. Note that the field inside the slot is only amplified for the symmetric case.

$$E_x = E_0 \begin{cases} n_{\mathrm{eff},z}\cos(-0.5k_x L_{\mathrm{lateral}} + \varphi)\Theta(x), & 0 < x < 0.5w_{\mathrm{slot}} \\ (n_{\mathrm{eff},z}/\varepsilon_x)\cos(k_x(x - 0.5(L_{\mathrm{lateral}} + w_{\mathrm{slot}}) + \varphi), & 0.5w_{\mathrm{slot}} < x < 0.5w_{\mathrm{slot}} + L_{\mathrm{lateral}}, \\ n_{\mathrm{eff},z}\cos(0.5k_x L_{\mathrm{side}} + \varphi)\exp(-\gamma(x - 0.5w_{\mathrm{slot}} - L_{\mathrm{lateral}})), & x > 0.5w_{\mathrm{slot}} + L_{\mathrm{lateral}} \end{cases} \quad (4)$$

where φ is the phase shift at the middle of each slab metal–dielectric layer pair region that arises from the mode coupling, $\gamma = (k_0^2 - k_z^2)^{0.5}$ is the field decay rate in the silica (k_z is the wave-vector in the propagation direction and k_0 is the wave vector for free space), and $\Theta(x)$ is

$$\Theta(x) = \begin{cases} \cosh(\gamma x)/\cosh(0.5\gamma w_{\mathrm{slot}}) \\ \sinh(\gamma x)/\sinh(0.5\gamma w_{\mathrm{slot}}) \end{cases}, \quad (5)$$

where the first line corresponds to symmetric modes and the second line corresponds to antisymmetric modes. The values of the electric field on the opposite sides of the slot (i.e., in the negative x direction) are exactly the same for symmetric modes and have the opposite sign for antisymmetric modes.

3. SLOT WAVEGUIDE ANALYSIS

The optical properties of the layered slot waveguide have been studied by calculating the modal effective refractive index $n_{\mathrm{eff},z} = k_z/k_0$ for the symmetric quasi-TE_{00} mode, using COMSOL Multiphysics finite element method software [37]. The waveguide geometry was simulated as an x–y profile and semi-infinite in the z direction. The slab metal–dielectric regions had a height of $H = 250$ nm and a width of $L_{\mathrm{lateral}} = 320$ nm. The structure was embedded in a background silica medium with dimensional size of 1.5 by 1.5 μm and was surrounded by perfectly matched layers (PMLs). This waveguide geometry is capable of supporting different mode orders: quasi-TE_{00}, quasi-TE_{01}, quasi-TE_{02}, and quasi-TE_{03} modes are plotted in Fig. 4.

We begin our discussion of the propagation problem by considering the fundamental quasi-TE_{00} [Fig. 4(a)] and varying the metal layer/dielectric layer thickness ratio for a fixed gap width of 20 nm and wavelengths covering the range from 1.39 to 1.7 μm. The calculated effective mode indices are plotted in Fig. 5 (real part) and Fig. 6 (imaginary part) using the following notation: no additional symbol is used for 25 nm/0 nm (only silver), • is used for 20 nm/5 nm, ○ is used for 15 nm/10 nm, × is used for 10 nm/15 nm, Δ is used for 7.5 nm/17.5 nm, ∇ is used for 5 nm/20 nm, and □ is used for 0 nm/25 nm (only silicon). The modal effective refractive index gradually increased as the volume fraction of dielectric material (i.e., silicon) became larger, which may be attributed to the slot waveguide resonance that arose from the enhanced field coupling inside the lateral slab regions. On the other hand, $n_{\mathrm{eff},z}$ decreased with increasing metallic fraction and demonstrated a tendency to match the properties of a purely silver plasmonic slot waveguide. It is possible to achieve even higher values of modal effective refractive index by using very thin silver films, but, as a trade-off, the imaginary part of $n_{\mathrm{eff},z}$ will also become larger, thereby increasing the propagation losses.

We have also examined the slot waveguide effective indices for several different gap widths. The Ag/Si ratio was selected to be 15 nm/10 nm, and the distance between the two metal–dielectric slab regions was increased progressively from 10 to 300 nm, as shown in Fig. 7. As expected, the narrow gap of 10 nm had the highest modal effective refractive index of $n_{\mathrm{eff},z} = 4$, due to the strong field localization inside the slot region, while gaps wider than 140 nm showed poor confinement, since the structure effectively transformed into two weakly coupled, finite-width slab waveguides. For this case, the further reduction of the modal effective refractive index of the silica-filled slot is explained by its gradual approach to the refractive index of a bulk silica region, i.e., $n_{\mathrm{SiO_2}} = 1.444$.

The slot waveguide was studied for its dispersion properties, which were calculated via the dispersion coefficient defined by

$$D(\lambda) = -\frac{\lambda_0}{c}\frac{\partial^2 n_{\mathrm{eff},z}}{\partial \lambda_0^2}. \quad (6)$$

The dispersion coefficient, expressed in units of ps/(nm × km), for a 20 nm wide silica-filled slot, is shown in Fig. 8. All the silver/silicon thickness ratios have negative

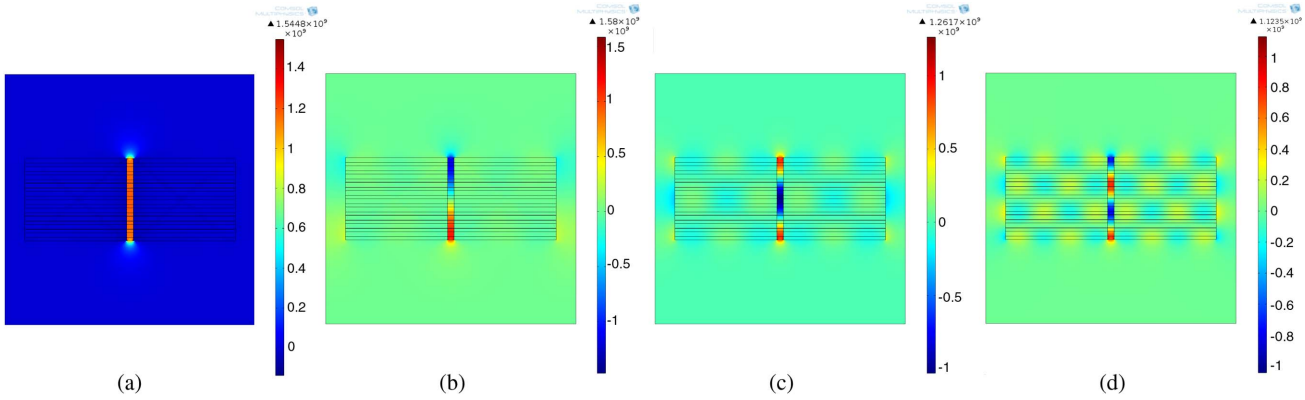

Fig. 4. (a) E_x profile for quasi-TE_{00} fundamental slot mode. (b) E_x profile for quasi-TE_{01} slot mode. (c) E_x profile for quasi-TE_{02} slot mode. (d) E_x profile for quasi-TE_{03} slot mode.

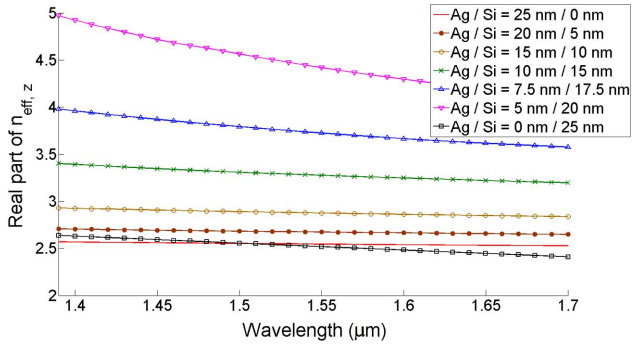

Fig. 5. Real part of modal effective refractive index.

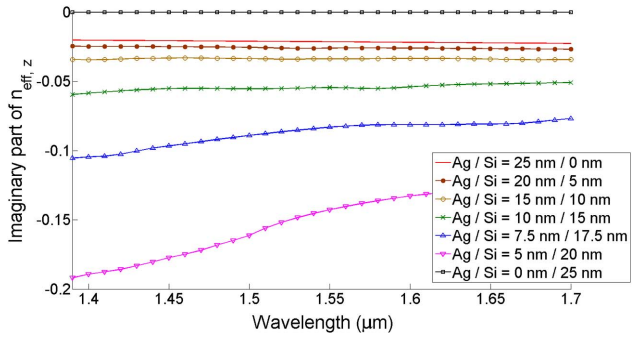

Fig. 6. Imaginary part of modal effective refractive index.

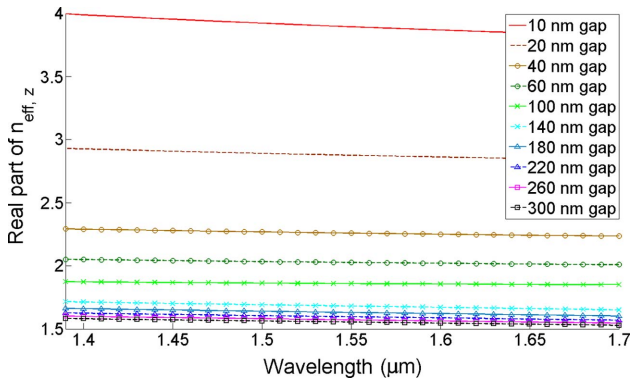

Fig. 7. Waveguide modal indices for different slot widths.

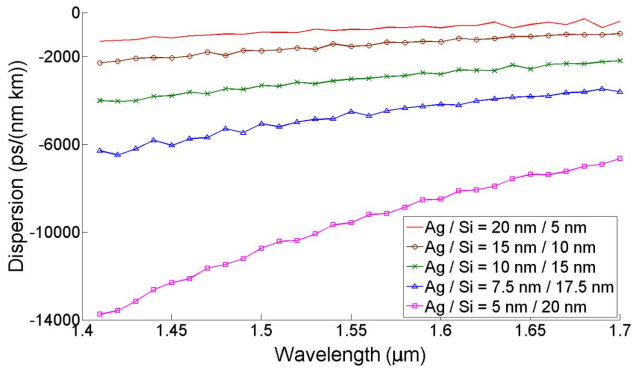

Fig. 8. Dispersion for waveguide with 20 nm slot width.

dispersion with magnitudes on the order of 10^4 ps/(nm × km) or lower. As mentioned earlier, larger values of the silicon fraction (such as Ag/Si ratio of 5 nm/20 nm) allowed stronger coupling between the modal electric field and the highly dispersive metallic regions, which resulted in higher magnitudes for the slot waveguide dispersion. The oscillations in the dispersion curves are attributed to round-off errors: The precision of the numerical calculation of $n_{\mathrm{eff},z}$ is four significant digits after the decimal point. Since no smoothing is performed for the effective refractive index data, possible numerical and round-off errors can accumulate, leading to random fluctuations in the calculation of the second derivative. Although the high dispersion magnitudes could be disadvantageous for some applications, the wave will decay to virtually zero before the group delay will affect the guided mode significantly.

Finally, for a slot waveguide with a gap width of 20 nm, a metal/dielectric ratio of 15 nm/10 nm, and at a wavelength of 1550 nm, the ratio of group delay $\Delta\tau$ to the spectral line width $\Delta\lambda$, calculated as $\Delta\tau/\Delta\lambda = D \times L_{\mathrm{propag}}$, was found to be -3.5×10^{-5} s/nm. In many applications, the variation of the group delay is not crucial, but it could become a problem in high-speed or broadband systems.

4. COUPLING STRIPE AND SLOT WAVEGUIDES

The slot waveguide can be coupled directly to a conventional stripe waveguide, but this may be very inefficient at infrared frequencies for nanometer scale slots, because of the large differences in the distributions of the optical modes [37]. One way to improve the coupling efficiency between two butted waveguides is to combine mutually complementary tapers [38]: the end of the input stripe waveguide is tapered and then inserted into the slot; the lateral regions of the slot waveguide are also tapered and are formed into a Y-shaped channel to fit the tapered end of the stripe waveguide (as shown schematically in Fig. 9). With reduction of the taper width, the light emitted by the stripe waveguide leaks into the two adjacent gaps between complementary tapers. As the wave propagates further, these gaps also become narrower and eventually merge to form a single slot.

The coupled waveguide was studied by commercial finite-difference time-domain software [39]. The quasi-TE_{00} wave originated at the beginning of the taper and propagated in the z direction, as shown in Fig. 9. The source has been positioned in the middle of the stripe waveguide cross section (in x–y plane) and had a chosen mode-field profile. The

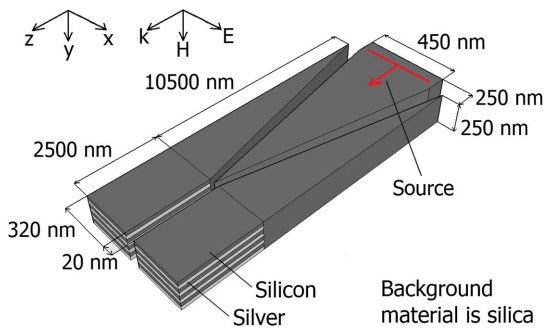

Fig. 9. Slot waveguide coupled with stripe waveguide.

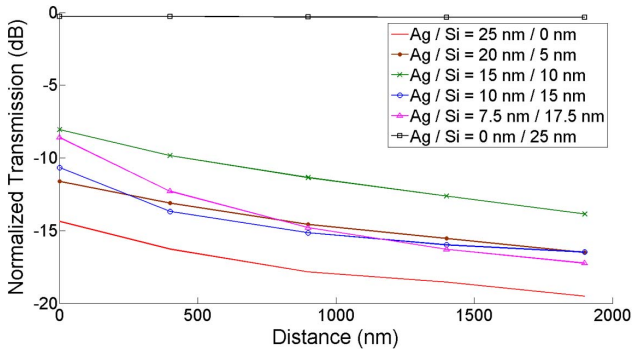

Fig. 10. Normalized transmission for the 20 nm gap width.

computational region was terminated by PMLs. The numerical mesh was set to be nonuniform, becoming denser close to the metal–dielectric interfaces. The grid sizes chosen for the silver regions were $\Delta x = \Delta y = \Delta z = 2.5$ nm, and the grid sizes for the silicon regions were $\Delta y = 2.5$ nm, $\Delta z = 100$ nm, and $\Delta x = 5$ nm. The results obtained from the use of finer meshes ($\Delta y = 1.25$ nm) were only 2% different from the results for the coarser mesh. However, the simulation memory requirements increased by a factor of 2. The calculation time step used in the simulations was 5×10^{-18} s, which was well below the stability limit. The material dispersion data was loaded from the built-in library of the software [40].

The input–output coupling efficiency is determined by the amount of transmitted power, which was measured at several points along the waveguide axis: (a) before the source; (b) immediately after the source; (c) at the end of the taper; and (d) equidistantly inside the slot waveguide. The calculated power level was then normalized with respect to the power recorded next to the source, and the geometrical dimensions of the structure were varied in order to find the maximum transmission. For a purely dielectric structure, almost 98% of the incident light was coupled into the slot waveguide. The remaining light mostly scattered back toward the source, and the normalized reflection level was only approximately 1%. The calculated transmitted power levels, as a function of the distance traveled, for the waveguide with a 20 nm wide silica-filled slot are shown in logarithmic scale in Fig. 10. The following notation applies: no additional symbol is used for 25 nm/0 nm (only silver), • is used for 20 nm/5 nm, × is used for 15 nm/10 nm, ○ is used for 10 nm/15 nm, Δ is used for 7.5 nm/17.5 nm, and □ is used for 0 nm/25 nm (only silicon). The highest power transmission was obtained for a purely silicon slot waveguide, while the lowest amount of power was transmitted in the MDM waveguide. For the slot waveguides with lateral slab regions formed by the hyperbolic metamaterial, the power was transmitted by both SPP propagation at the metamaterial–silica interfaces and by the fundamental slot-confined quasi-TE_{00} mode that originated from the lateral coupling between the silicon dielectric layers. Because of the high propagation losses, the SPP transmission components decayed rapidly for all samples (except for an Ag/Si ratio of 10 nm/15 nm), which resulted in the slot-confined mode being the primary mechanism of power transmission for distances over 1.5 μm. The Ag/Si ratio of 15–10 nm provided the smallest power attenuation of 13.85 dB, which may be attributed to the partial excitation of long-range SPPs that could propagate for distances of tens of micrometers before fading. The lower input values for the slot waveguides with silver inclusions (i.e., the insertion losses) are explained by the weaker coupling of light into them, since infrared radiation scattered more intensively from the metal–dielectric interface of the tapered region. The differences in the curve slopes for the silver/silicon ratios considered may be ascribed to the simultaneous excitation of higher order modes, in addition to the fundamental quasi-TE_{00} slot mode. However, the higher order modes decayed swiftly, due to the large imaginary part of the modal effective refractive indices, and their impact on the power transmission at distances greater than 1 μm became negligible.

To estimate the wave confinement inside the silica-filled slot waveguide, the electric field strength was compared for different silver/silicon layer thickness ratios. The modal E_x component was recorded at equidistantly spaced points over the x–y cross section, at the slot waveguide end. The field in the intermediate points was interpolated using cubic Hermite splines. The electric field distribution expressed on a logarithmic scale is shown in Figs. 11(a)–11(c) for a 20 nm slot width. The logarithmic values of E_x were normalized with respect to the highest logarithmic value in the middle of the slot. The confinement for the purely dielectric waveguide case [Fig. 11(a)] was not very strong: the electric field maximum was localized not only inside the slot, but also extended considerably into the adjacent lateral regions. The magnitude of the modal electrical field strength in the adjacent regions was approximately 20 times (in terms of absolute value) lower than the E_x magnitude for the field maximum inside the slot. The field distribution for a slot waveguide with a silver/silicon layer thickness ratio of 15 nm/10 nm showed better confinement [Fig. 11(b)]. Even though E_x was nonzero in the hyperbolic metamaterial lateral regions, it was less than 0.01% of the field maximum value inside the slot. Finally, for the purely MDM waveguide, the electric field was strongly

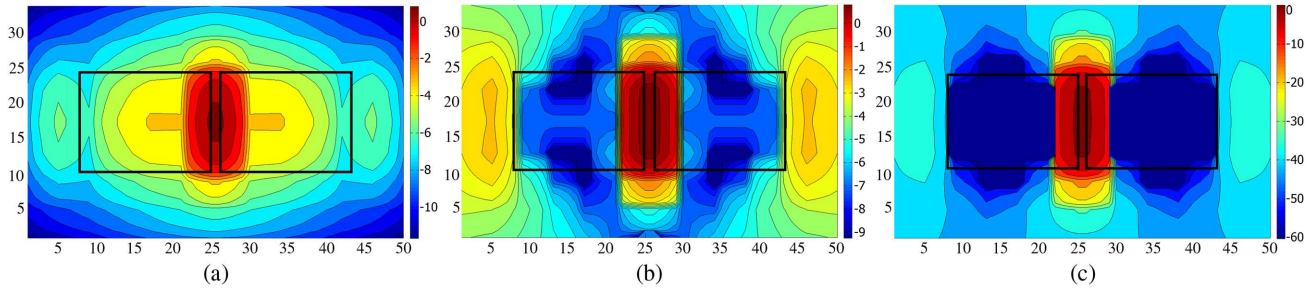

Fig. 11. (a) Normalized E_x profile in logarithmic scale for 0 nm/25 nm silver/silicon layer thickness ratio. (b) Normalized E_x profile in logarithmic scale for 15 nm/10 nm silver/silicon layer thickness ratio. (c) Normalized E_x profile in logarithmic scale for 25 nm/0 nm silver/silicon layer thickness ratio.

confined inside the slot, and no light penetrated significantly into the lateral slab regions [Fig. 11(c)].

5. CONCLUSIONS

In this paper, we have considered the silica-filled slot waveguide with lateral slab regions formed by alternating metal–dielectric multilayers. This structure was used for the subwavelength confinement of light in the silica-filled slot in the short-wavelength infrared region. Numerical simulations have shown that high modal effective indices can be obtained for propagating waves that have their main electric field component directed across the gap. The increase of the gap width resulted in the reduction of modal effective index and the waveguides with smaller volume amounts of metal showed to be more dispersive. The coupling from a conventional stripe waveguide has also been studied. We have obtained the highest transmitted power level for a coupled geometry with an Ag/Si ratio of 15 nm/10 nm, which was 3.5 times higher than for the MDM structure of the same dimensions. Finally, we have found that using hyperbolic metamaterials as a lateral cladding region for the silica-filled slot waveguide resulted in enhanced subwavelength confinement (99% greater than for a silicon only waveguide, in terms of the normalized electric field values inside the slot).

While guiding light over long distances (more than several micrometers) could be an important issue because of the intrinsic metallic propagation losses, the slot waveguide design that we have proposed has significant potential for the construction of photonic circuits and integrated devices such as micro-lasers or nanoantennas. These miniature waveguides can confine light in a very small transversal region (less than 100 nm) and could be used in the fabrication of very compact devices (with typical lengths of less than 1 μm) such as short-distance optical interconnects, modulators, switches, and couplers. Other possible applications could include optical trapping, nonlinear optical devices, and dispersion compensation for sufficiently high power modes.

REFERENCES

1. D. Liu and C. Svensson, "Power consumption estimation in CMOS VLSI circuit," IEEE J. Solid-State Circuits **29**, 663–670 (1994).
2. S. Fan, P. R. Villeneuve, and J. D. Joannopoulos, "Channel drop filters in photonic crystals," Opt. Express **3**, 4–11 (1998).
3. T. Asano, M. Mochizuki, S. Noda, M. Okano, and M. Imada, "A channel drop filter using a single-defect in a 2-D photonic crystal slab: defect engineering with respect to polarization mode and ratio of emissions from upper to lower sides," J. Lightwave Technol. **21**, 1370–1376 (2003).
4. H. Nguyen, N. Yazawa, S. Hashimoto, S. Otsuka, and T. Baba, "Sub-100 μm photonic crystal Si optical modulators: spectral, athermal, and high speed performance," IEEE J. Sel. Top. Quantum Electron. **19**, 3400811 (2013).
5. H. T. Hattori, V. M. Schneider, and O. Lisboa, "Cantor set fiber Bragg grating," J. Opt. Soc. Am. A **17**, 1583–1589 (2000).
6. T. F. Krauss, R. M. De La Rue, and S. Brand, "Two-dimensional photonic bandgap structures at near infrared wavelength," Nature **383**, 699–702 (1996).
7. H. T. Hattori, I. McKerracher, H. H. Tan, C. Jagadish, and R. M. De La Rue, "In-plane coupling of light from InP-based photonic crystal band-edge lasers into single-mode waveguides," IEEE J. Quantum Electron. **43**, 279–286 (2007).
8. M. Fujita, A. Sakai, and T. Baba, "Ultra-small and ultra-low threshold microdisk injection laser: design, fabrication, lasing characteristics and spontaneous emission factor," IEEE J. Sel. Top. Quantum Electron. **5**, 673–681 (1999).
9. S. V. Boriskina, T. M. Benson, P. D. Sewell, and A. I. Nosich, "Directional emission, increased free spectral range, and mode Q-factors in 2-D wavelength-scale optical microcavity structures," IEEE J. Sel. Top. Quantum Electron. **12**, 1175–1182 (2006).
10. H. T. Hattori, "Analysis of optically pumped equilateral triangular microlasers with three mode-selective trenches," Appl. Opt. **47**, 2178–2185 (2008).
11. H. T. Hattori, D. Liu, H. H. Tan, and C. Jagadish, "Large square resonator laser with quasi single-mode operation," IEEE Photon. Technol. Lett. **21**, 359–361 (2009).
12. S. E. Kocabas, G. Veronis, D. A. B. Miller, and S. Fan, "Modal analysis and coupling in metal-insulator-metal waveguides," Phys. Rev. B **79**, 035120 (2009).
13. H. J. Lezec, A. Degiron, E. Devaux, R. A. Linke, L. Martin-Moreno, F. J. Garcia-Vidal, and T. W. Ebbesen, "Beaming light from a subwavelength aperture," Science **297**, 820–822 (2002).
14. S. A. Maier, P. G. Kik, H. A. Atwater, S. Meltzer, E. Harel, B. E. Koel, and A. A. G. Requicha, "Local detection of electromagnetic energy transport below the diffraction limit in metal nanoparticle plasmon waveguides," Nat. Mater. **2**, 229–232 (2003).
15. J. Lin, J. P. B. Mueller, Q. Wang, G. Yuan, N. Antoniou, X. C. Yuan, and F. Capasso, "Polarization-controlled tunable directional coupling of surface plasmon polaritons," Science **340**, 331–334 (2013).
16. M. T. Hill, E. M. Marell, S. P. Leong, B. Smalbrugge, Y. Zhu, M. Sun, P. J. van Veldhoven, E. J. Geluk, F. Karouta, Y. S. Oei, R. Nötzel, C. Z. Ning, and M. K. Smit, "Lasing in metal-insulator-metal sub-wavelength plasmonic waveguides," Opt. Express **17**, 11107–11112 (2009).
17. E. Cubukcu, N. Yu, E. J. Smythe, L. Diehl, K. B. Crozier, and F. Capasso, "Plasmonic laser antennas and related devices," IEEE J. Sel. Top. Quantum Electron. **14**, 1448–1461 (2008).
18. H. T. Hattori, Z. Li, D. Liu, I. D. Rukhlenko, and M. Premaratne, "Coupling of light from microdisk lasers into plasmonic nanoantennas," Opt. Express **17**, 20878–20884 (2009).
19. E. G. Mironov, Z. Li, H. T. Hattori, K. Vora, H. H. Tan, and C. Jagadish, "Titanium nano-antenna for high-power pulsed operation," J. Lightwave Technol. **31**, 2459–2466 (2013).
20. H. J. Y. Allen, S. D. Moore, B. S. Schmidt, M. Klug, M. Lipson, and D. Erickson, "Optical manipulation of nanoparticles and biomolecules in sub-wavelength slot waveguides," Nature **457**, 675–677 (2009).
21. A. N. Grigorenko, N. W. Roberts, M. R. Dickinson, and Y. Zhang, "Nanometric optical tweezers based on nanostructured substrates," Nat. Photonics **2**, 365–370 (2008).
22. J. Van Campehout, P. R. A. Binetti, P. R. Romeo, P. Regreny, C. Seassal, X. J. M. Leijtens, T. De Vries, Y. S. Oei, R. P. J. Van Veldhove, R. Nötzel, L. Di Cioccio, J. M. Fedeli, M. K. Smit, D. Van Thourhout, and R. Baets, "Low-footprint optical interconnect on an SOI chip through heterogeneous integration of InP-Based microdisk lasers and microdetectors," IEEE Photon. Technol. Lett. **21**, 522–524 (2009).
23. L. O'Faolain, X. Yuan, D. McIntyre, S. Thoms, H. Chong, R. M. De La Rue, and T. F. Krauss, "Low-loss propagation in photonic crystal waveguides," Electron. Lett. **42**, 1454–1455 (2006).
24. M. Gnan, S. Thoms, D. S. Macintyre, R. M. De La Rue, and M. Sorel, "Fabrication of low-loss photonic wires in silicon-on-insulator using hydrogen silsesquioxane electron-beam resist," Electron. Lett. **44**, 115–116 (2008).
25. G. Roelkens, D. Van Thourhout, and R. Baets, "High efficiency grating coupler between silicon-on-insulator waveguides and perfectly vertical optical fibers," Opt. Lett. **32**, 1495–1497 (2007).
26. Y. He, S. He, J. Gao, and X. Yang, "Nanoscale metamaterial optical waveguides with ultrahigh refractive indices," J. Opt. Soc. Am. B **29**, 2559–2566 (2012).
27. L. Chen, J. Shakya, and M. Lipson, "Subwavelength confinement in an integrated metal slot waveguide on silicon," Opt. Lett. **31**, 2133–2135 (2006).
28. G. Veronis and S. Fan, "Modes of subwavelength plasmonic slot waveguides," J. Lightwave Technol. **25**, 2511–2521 (2007).

29. J. A. Dionne, H. J. Lezec, and H. A. Atwater, "Highly confined photon transport in subwavelength metallic slot waveguides," Nano Lett. **6**, 1928–1932 (2006).
30. V. R. Almeida, Q. Xu, C. A. Barrios, and M. Lipson, "Guiding and confining light in void nanostructure," Opt. Lett. **29**, 1209–1211 (2004).
31. J. J. Burke, G. I. Stegeman, and T. Tamir, "Surface-polariton-like waves guided by thin, lossy metal films," Phys. Rev. B **33**, 5186–5201 (1986).
32. P. Berini, "Plasmon-polariton waves guided by thin lossy metal films of finite width: bound modes of symmetric structures," Phys. Rev. B **61**, 10484–10503 (2000).
33. C. A. Foss, G. L. Hornyak, J. A. Stockert, and C. R. Martin, "Template-synthesized nanoscopic gold particles: optical spectra and the effects of particle size and shape," J. Phys. Chem. **98**, 2963–2971 (1994).
34. A. Sihvola, *Electromagnetic Mixing Formulas and Applications* (Institution of Electrical Engineering, 1999).
35. P. U. Jepsen, B. M. Fischer, A. Thoman, H. Helm, J. Y. Suh, R. Lopez, and R. F. Haglund, Jr., "Metal-insulator phase transition in a VO_2 thin film observed with terahertz spectroscopy," Phys. Rev. B **74**, 205103 (2006).
36. P. B. Johnson and R. W. Christy, "Optical constants of the noble metals," Phys. Rev. B **6**, 4370–4379 (1972).
37. COMSOL Multiphysics 4.3a [Online]. Available: http://www.comsol.com.
38. Q. Xu, V. R. Almeida, P. R. Panepucci, and M. Lipson, "Experimental demonstration of guiding and confining light in nanometer-size low-refractive-index material," Opt. Lett. **29**, 1626–1628 (2004).
39. Z. Wang, N. Zhu, Y. Tang, L. Wosinski, D. Dai, and S. He, "Ultracompact low-loss coupler between strip and slot waveguides," Opt. Lett. **34**, 1498–1500 (2009).
40. Fullwave 6.0 RSOFT Design Group, 1999, [Online]. Available: http://www.rsoftdesign.com.